Oxygen-Evolution Catalysts

Deutsche Ausgabe: DOI: 10.1002/ange.201504358
Internationale Ausgabe: DOI: 10.1002/anie.201504358

Synergistic Effect between Metal–Nitrogen–Carbon Sheets and NiO Nanoparticles for Enhanced Electrochemical Water-Oxidation Performance**

*Jun Wang, Kai Li, Hai-xia Zhong, Dan Xu, Zhong-li Wang, Zheng Jiang, Zhi-jian Wu, and Xin-bo Zhang**

Abstract: *Identifying effective means to improve the electrochemical performance of oxygen-evolution catalysts represents a significant challenge in several emerging renewable energy technologies. Herein, we consider metal–nitrogen–carbon sheets which are commonly used for catalyzing the oxygen-reduction reaction (ORR), as the support to load NiO nanoparticles for the oxygen-evolution reaction (OER). FeNC sheets, as the advanced supports, synergistically promote the NiO nanocatalysts to exhibit superior performance in alkaline media, which is confirmed by experimental observations and density functional theory (DFT) calculations. Our findings show the advantages in considering the support effect for designing highly active, durable, and cost-effective OER electrocatalysts.*

The ever-growing public concerns about the energy crisis and energy security call for the development of sustainable energy as viable alternatives to fossil fuels.[1] Solar energy has the potential to meet global energy demand for clean and renewable energy, provided its conversion and storage issues are settled.[2] The electrochemical splitting of water offers a promising process enabling the conversion from solar to storable hydrogen fuels.[3] In this process, the oxygen-evolution reaction (OER) is a kinetic barrier, requiring a large overpotential that deteriorates the overall efficiency of water splitting.[4] At present, ruthenium and iridium oxides are regarded as the benchmarking OER catalysts, but the high cost and low abundance impede their use on a large scale.[5] Therefore, the exploration of active, durable, and inexpensive first-row transition-metal oxides (MOs) with commensurate OER performance is highly pursued.[6] Among them, nickel-based oxides have been proposed as good candidates and many efforts have focused on identifying means to further improve their performance.[7]

Besides tuning the size, shape, composition, and crystallinity of active component of catalysts,[8] optimizing the interaction between the active component and the support could boost the catalytic performance. This is because the support could raise the dispersity of the active sites, facilitating the mass-transport and electron-transfer kinetics.[9] Incorporating active materials with functional supports has been shown to be an effective means of raising the activity of OER catalysts.[6e,7a,10] For instance, Dai and co-workers found that the enhanced OER activity of Co_3O_4 nanoparticles (NPs) was obtained by anchoring them on nitrogen-doped graphene.[10c] Other reports also showed that manganese, cobalt, and nickel oxides deposited on noble metals can exhibit superior OER activities in contrast to their support-free counterparts.[6e,7a,10d] The substantial enhancement is believed to originate from the synergetic effect between the metal oxides and the supports.

Metal–nitrogen–carbon (MNC) materials, in which the metal is either Fe and/or Co, are emerging as the most promising oxygen-reduction catalysts.[11] And the active sites are ascribed to central metal ions stabilized by nitrogen functional groups on carbonaceous surfaces, showing distinct interactions with oxygen molecules and the intermediates.[11,12] Furthermore, the introduction of heteroatoms tunes the electron-donating/withdrawing capability of the carbon basal plane. These unique properties theoretically suggest that MNC materials are potential catalyst supports. Inspired by these ideas, herein, as a proof-of-concept experiment, we first take NiO as active component to evaluate the support effect of MNC sheets. Impressively, the FeNC sheets/NiO exhibits excellent OER performance including high activity and long term stability.

As presented in Scheme 1, the synthesis begins by coating graphene oxide (GO) sheets with polydopamine (PDA) which can deposit on virtually any surface through the self-polymerization of dopamine in an alkaline environment and can subsequently chelate with many types of metal ions.[13] Thus the GO@PDA sheets are impregnated with Fe and Co

[*] J. Wang,[+] K. Li,[+] H.-x. Zhong, D. Xu, Z.-l. Wang, Prof. Dr. Z.-j. Wu, Prof. Dr. X.-b. Zhang
State Key Laboratory of Rare Earth Resource Utilization
Changchun Institute of Applied Chemistry
Chinese Academy of Sciences
Changchun, 130022 (P.R. China)
E-mail: xbzhang@ciac.ac.cn
J. Wang,[+] H.-x. Zhong
University of Chinese Academy of Sciences
Beijing, 100049 (P.R. China)
Prof. Dr. Z. Jiang
Shanghai Synchrotron Radiation Facility, Shanghai Institute of Applied Physics, Chinese Academy of Sciences
Shanghai, 201204 (China)
[+] These authors contributed equally to this work.

[**] The authors greatly appreciate the referee for the very constructive comments and insightful suggestions on this manuscript. This work is financially supported by National Program on Key Basic Research Project of China (973 Program, Grant No. 2012CB215500 and 2014CB932300), National Natural Science Foundation of China (Grant No. 21422108, 21471146, and 51472232).
Supporting information for this article is available on the WWW under http://dx.doi.org/10.1002/anie.201504358.

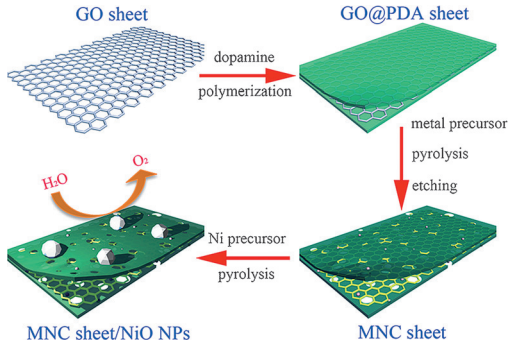

Scheme 1. Schematic illustration of the synthesis of metal–nitrogen–carbon (MNC) sheet/NiO NPs.

precursors which after heat-treatment and acid-leaching give Fe–nitrogen–carbon (FeNC) and Co–nitrogen–carbon (CoNC) sheets, respectively. Metal-free NC sheets are also prepared as the control sample by heat-treating GO@PDA sheets directly. After loading the sheets with NiO NPs to perform OER, the FeNC sheets display the most improved performance which is a result of the low electron-transfer barrier and high electron-coupling capability.

The morphology of GO@PDA sheets was first investigated by transmission electron microscopy (TEM). As shown in Figure 1 a, several thick and wrinkled sheets with smooth surface and sizes on the micrometer scale are observed. And no isolated PDA NPs appear, suggesting the completely selective polymerization of dopamine on the GO surface. When converted into FeNC sheets, though their surfaces becomes rough, the structural integrity of sheet is well preserved (Figure 1 b). The highly magnified TEM image reveals that the surface of the FeNC sheets is composed of many mesopores which are derived from the unstable Fe species after acid-leaching (Figure 1 c). The porous character will clearly increase the surface area and facilitate gas diffusion, thus boosting the activity of the catalyst. Meanwhile, a few of residual Fe NPs are also observed with a spacing of 0.202 nm which can be assigned to Fe(110) plane. Fourier-transform infrared (FT-IR) spectra illustrate that the characteristic peaks of several functional groups belonging to PDA disappear from the surface of FeNC sheets after heat-treatment (Figure 1 d). Meanwhile the thickness of FeNC sheets (ca. 1.5 nm) shrinks in comparison to that of GO@PDA sheets (ca. 3.5 nm), as confirmed by atomic force microscopy (AFM) images (Figure S1 in the Supporting Information). The X-ray diffraction patterns (XRD) display two peaks centered at approximately 25° and 44°, corresponding to carbon (002) and (101) diffractions for FeNC sheets, in contrast with one broad peak for GO@PDA, indicative of the high graphitic degree of the FeNC sheets (Figure 1 l). Similar TEM, FT-IR, AFM and XRD results are observed for CoNC and NC sheets, except for the relatively smooth surface of NC sheets (Figure S2–S6).

Furthermore, the Brunauer–Emmett–Teller (BET) surface areas of the three samples are estimated by N_2 adsorption–desorption isotherms (Figure S7 a). The BET surface areas and pore volumes are found to be 439 $m^2 g^{-1}$ and 0.44 $cm^3 g^{-1}$ for FeNC sheets, 513 $m^2 g^{-1}$ and 1.00 $cm^3 g^{-1}$ for CoNC sheets, and 323 $m^2 g^{-1}$ and 0.20 $cm^3 g^{-1}$ for NC sheets, respectively. The pore size distribution reveals that CoNC sheets have more mesopores than FeNC and NC sheets (Figure S7 b). Reasonably, NC sheets without porous surface take the lowest BET surface area and pore volume. However, their discrepancies between FeNC and CoNC sheets are inscrutable, which may be explained by their compositions.

To this end, X-ray photoelectron spectroscopy (XPS) was performed on FeNC, CoNC and NC sheets. As shown in Figure S8, the three samples are all composed of C, N, and O. And the characteristic peaks of Fe and Co are also observed for FeNC and CoNC sheets, respectively. These results are further corroborated by energy dispersive spectroscopy (Figure S9). Element mapping images reflect that all the samples have the homogeneous distribution of C, N, and O in their sheet structure. Besides, small amounts of Fe and Co are present in the FeNC and CoNC sheets, respectively (Figure 1 e–i and Figure S2–S3). The atomic ratios of Fe and Co are 0.10 % and 0.04 % (Table S1), consistent with inductively coupled plasma-atomic emission spectroscopy measurements wherein the detected Fe and Co contents are 8892 and 3779 ppm, respectively.

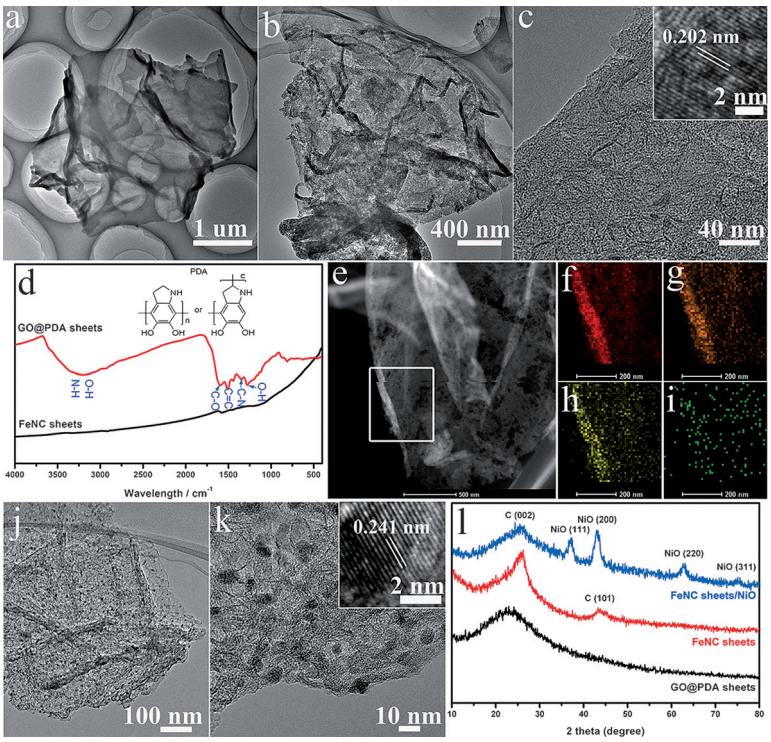

Figure 1. TEM images of a) GO@PDA and b,c) FeNC sheets; d) FT-IR spectra of GO@PDA and FeNC sheets; e) HAADF-STEM image of FeNC sheets and the corresponding element-mapping images of f) C, g) N, h) O, and i) Fe; j),k) TEM images of FeNC sheets/NiO; l) XRD patterns of GO@PDA sheets, FeNC sheets, and FeNC sheets/NiO.

Additionally, the Raman spectra reveal that FeNC sheets have the lowest I_D/I_G ratio (Figure S10), implying the relatively low structural defects, which is also verified by the lowest (N + O)/C ratio of FeNC sheets (3.81 %) in contrast to that of CoNC (4.33 %) and NC (8.06 %) sheets (Table S1). Conclusively, the reason for low BET surface area and pore volume of FeNC sheets, in comparison to that of CoNC sheets, may be ascribed to the high residual Fe content and low number of defect sites.

Deposition of NiO NPs on the three supports is easily achieved by the impregnation and pyrolysis process. For a full comparison, graphene (G) sheets were selected as another support and pure NiO NPs with uneven size distribution were obtained by pyrolyzing nickel acetate directly (Figure S11). The NPs with sizes ranging from 5 to 8 nm are fairly well dispersed on FeNC and CoNC sheets (Figure 1 j,k and Figure S2 h,i). However, a little agglomeration of the NPs happens on NC and G sheets, which may be caused by the smooth surface (Figure S3 g and Figure S11 b). The high-resolution TEM image shows the resolved lattice fringes of NiO(111) plane with a spacing of 0.241 nm. XRD patterns confirm the (111), (200), (220), and (311) diffractions of NiO (PDF#65-2901) as well (Figure 1 l and Figure S6).

The OER activities are characterized in a three-electrode electrochemical cell with a rotating disk electrode (RDE) configuration. Cyclic voltammetry (CV) is performed in 0.1 M KOH using a scan rate of 10 mV s^{-1}, at room temperature. Potentials are converted to the reversible hydrogen electrode (RHE) scale by calibration (Figure S12). Figure 2 a shows that the FeNC sheets/NiO displays greater current density and a more negative OER onset potential (1.47 V vs. RHE) than the CoNC sheets/NiO (1.49 V) and NC sheets/NiO (1.51 V). In addition, the overpotential required at the current density of 10 mA cm^{-2} is always regarded as the benchmark to estimate the activity of OER catalyst. The FeNC sheets/NiO and CoNC sheets/NiO reach this value with a potential of 1.62 and 1.64 V, respectively. Of note, G sheets/NiO and pure NiO show weak OER activities and the supports have little activity contribution. Figure 2 b reveals that Tafel slope of FeNC sheets/NiO is approximately 76 mV/decade, which is smaller than that of CoNC sheets/NiO and NC sheets/NiO, indicating the higher OER kinetics. The surface concentration of redox active Ni centers on the electrode can be extracted from the slope of the linear relationship between the peak current of the reduction wave and scan rate.[14] Therefore, the coverage of redox active Ni centers is calculated to be 51.94, 60.52, and 40.55 nmol cm^{-2} for FeNC sheets/NiO, CoNC sheets/NiO and NC sheets/NiO, respectively (Figure S13). In view of the fact that OER occurs only on the surface of the catalyst, these values represent the upper limits to the real number of catalytic sites. Thus, the lower turnover frequency (TOF) limit associated with FeNC sheets/NiO at $\eta = 350$ mV is 0.2 s^{-1}, which is higher than that of CoNC sheets/NiO (9.5×10^{-2} s^{-1}) and NC sheets/NiO (8.5×10^{-2} s^{-1}), highlighting the most positive effect of FeNC sheets in promoting OER activity. Based on these results, the FeNC sheets/NiO exerts high OER activity which is comparable to commercial RuO_2 (Figure S14) and many non-precious-metal-based catalysts (Table S2).[6a,b,7f,10b,c,14,15]

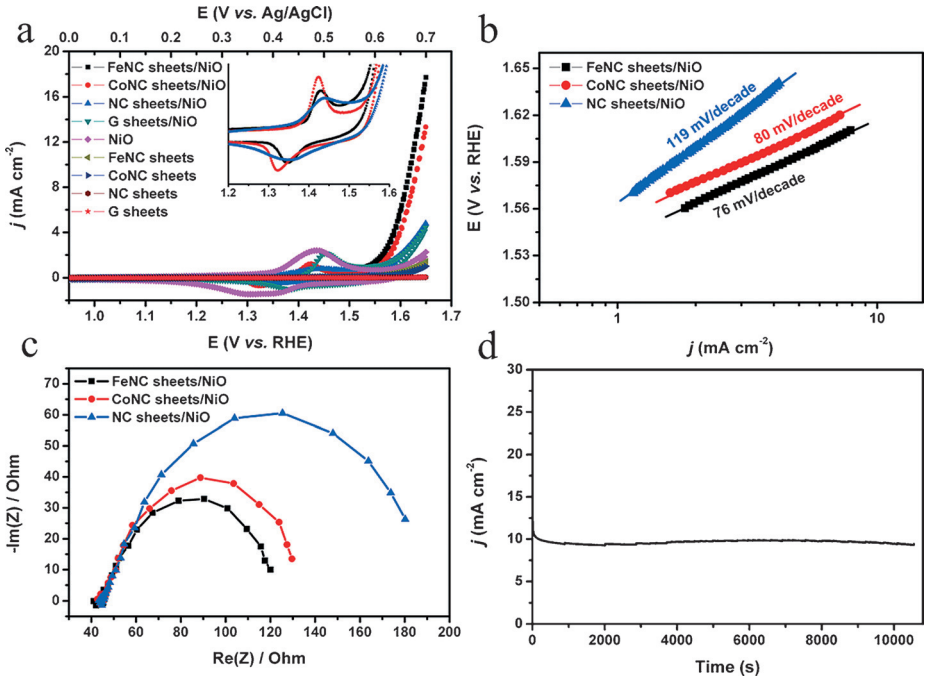

Figure 2. a) CV curves for OER on FeNC, CoNC, NC, and G sheets with and without NiO NPs at a scan rate of 10 mV s^{-1}; b) the corresponding Tafel plots; c) the electrochemical impedance plots obtained at a potential of 1.62 V vs. RHE; and d) a chronoamperometric test for OER over the FeNC sheets/NiO catalyst at 1.62 V vs. RHE. All the measurements are performed in 0.1 M KOH at room temperature with RDE rotation speed of 1000 rpm. Catalyst loading: approximately 0.24 mg cm^{-2}.

The electrochemical impedance spectroscopy (EIS) technique is used to provide deep insight into the kinetics during OER process. As shown in Figure 2 c, a lowest charge-transfer resistance is observed for FeNC sheets/NiO, associated with its superior OER activity. As the supports, CoNC and NC sheets have more defect sites, resulting in higher charge-transfer barrier at OER condition and thus inferior activities of the catalysts. Consequently, the good electron-transfer kinetics is a prime requirement for electrocatalyst to exhibit high activity. To assess the OER stability of FeNC sheets/NiO, a chronoamperometric test is carried out. Figure 2 d reveals that a strong activity maintenance over 10000 s is obtained at approximately 10 mA cm^{-2} with the applied potential of 1.62 V, suggesting the long-term durability.

The interaction between the supports and NiO NPs is analyzed by XPS spectra, in which the

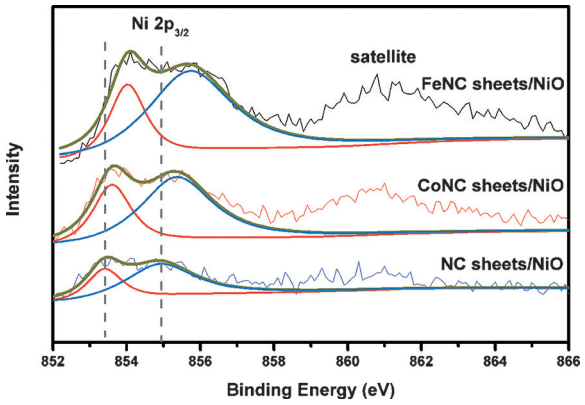

Figure 3. Ni $2p_{3/2}$ region of XPS spectra for NiO NPs supported on FeNC, CoNC, and NC sheets.

$Ni\,2p_{3/2}$ region can be deconvoluted into two peaks (Figure 3).[16] For NC sheets/NiO, the binding energies are located at 853.4 and 854.9 eV, which shift to higher values for CoNC sheets/NiO (853.6 and 855.4 eV) and FeNC sheets/NiO (854 and 855.7 eV). The X-ray absorption near-edge structure (XANES) spectra of these samples show the Ni K-edge of the FeNC sheets/NiO shifts to relatively higher energy, indicating the increased oxidation state of Ni atoms (Figure S15).[17] These phenomena demonstrate that FeNC sheets have the stronger electron coupling effect that facilitates electron transfer from NiO NPs to FeNC sheets. Previous work has indicated that the formation of the O–O bond in OOH adsorbate (Step 3, Figure 4) and the deprotonation of the oxyhydroxide group (Step 4, Figure 4) determine the electrocatalytic efficiency of OER.[4a] For the FeNC sheets/NiO, the NiO NPs, as electron donors, become more electrophilic, facilitating the nucleophilic reaction by OH^- with the intermediates and thus accelerating OER. Moreover, according to the Lewis acid–base concept, the electron donation from NiO NPs to FeNC sheets makes the NiO NPs more acidic, which will benefit the interaction with OH^-, leading to the improved OER activity. These results highlight the synergetic effect between FeNC sheets and NiO NPs.

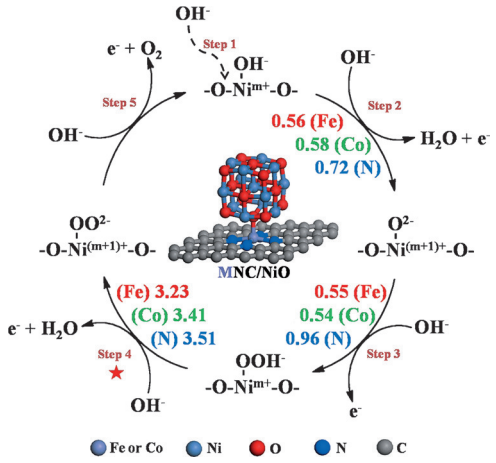

Figure 4. Schematic illustration of the OER pathways. The colored numbers are the kinetic energy barriers.

To confirm the experimental observations, density functional theory (DFT) calculation is employed to provide deeper insights into the detailed OER pathways (see calculation details in Supporting Information). As shown in Figure 4, FeNC/NiO and CoNC/NiO display no obvious discrepancy in the kinetic energy barriers for Step 2 and 3. However, the energy barrier of the rate determining step (Step 4) on FeNC/NiO is 3.23 eV, which is significantly lower than that of CoNC/NiO (3.41 eV). NC/NiO has the highest energy barriers for Steps 2–4, indicative of its unfavorable OER kinetics. Overall, these results are in agreement with the experimental observations, validating the speculations from XPS and XANES results and the superior promoting effect of the FeNC sheets.

To evaluate the Faradaic yield for OER, the FeNC sheets/NiO catalyst is loaded onto carbon paper (CP) and tested at a constant potential. Synchronously, the evolved gas during the reaction is monitored volumetrically using a gas burette at room temperature and atmospheric pressure. As shown in Figure S16, a 97 % Faradaic yield is estimated based on the observed gas volume and the theoretical gas volume calculated by the charge passed through the electrode. The 3 % loss may be ascribed to the dissolved gas in the electrolyte and the attached bubbles on electrode surface. Mass spectrum reveals that the evolved gas is composed of only O_2 and H_2. And a 22 h chronoamperometric test on the CP electrode shows no activity decrease, confirming the stability of the FeNC sheets/NiO catalyst (Figure S17).

In summary, we have investigated MNC sheets as the supports for NiO nanocatalysts for the OER, in which the FeNC sheets promote the catalysts to exhibit both high activity and long-term stability in alkaline medium. The experimental observations and DFT calculations confirm that the activity improvement originates from low electron-transfer barrier and high electron-coupling capability of the FeNC sheets, highlighting the synergistic effect between the FeNC sheets and NiO NPs. Our findings show the support effect should be considered when designing advanced and cost-effective OER electrocatalysts, which may find applications in energy conversion technologies including not only alkaline water electrolyzers but also metal–air batteries.

Keywords: electrocatalysis · metal–nitrogen–carbon sheets · nanoparticles · oxygen-evolution reaction · synergistic effect

How to cite: *Angew. Chem. Int. Ed.* **2015**, *54*, 10530–10534
Angew. Chem. **2015**, *127*, 10676–10680

[1] a) J. Chow, R. J. Kopp, P. R. Portney, *Science* **2003**, *302*, 1528; b) N. S. Lewis, D. G. Nocera, *Proc. Natl. Acad. Sci. USA* **2006**, *103*, 15729; c) S. Guo, S. Zhang, S. Sun, *Angew. Chem. Int. Ed.* **2013**, *52*, 8526; *Angew. Chem.* **2013**, *125*, 8686; d) M. Chhowalla, H. S. Shin, G. Eda, L. J. Li, K. P. Loh, H. Zhang, *Nat. Chem.* **2013**, *5*, 263; e) X. Ge, L. Chen, L. Zhang, Y. Wen, A. Hirata, M. Chen, *Adv. Mater.* **2014**, *26*, 3100; f) J. Lu, P. Zhang, A. Li, F. Su, T. Wang, Y. Liu, J. Gong, *Chem. Commun.* **2013**, *49*, 5817.

[2] a) T. R. Cook, D. K. Dogutan, S. Y. Reece, Y. Surendranath, T. S. Teets, D. G. Nocera, *Chem. Rev.* **2010**, *110*, 6474; b) A. J. Bard, M. A. Fox, *Acc. Chem. Res.* **1995**, *28*, 141; c) M. Grätzel, *Nature* **2001**, *414*, 338.

[3] a) M. G. Walter, E. L. Warren, J. R. McKone, S. W. Boettcher, Q. Mi, E. A. Santori, N. S. Lewis, *Chem. Rev.* **2010**, *110*, 6446; b) R. Subbaraman, D. Tripkovic, D. Strmcnik, K. C. Chang, M. Uchimura, A. P. Paulikas, V. Stamenkovic, N. M. Markovic, *Science* **2011**, *334*, 1256; c) D. G. Nocera, *Acc. Chem. Res.* **2012**, *45*, 767; d) M. H. V. Huynh, T. J. Meyer, *Chem. Rev.* **2007**, *107*, 5004; e) S. Hammes-Schiffer, *Acc. Chem. Res.* **2009**, *42*, 1881.

[4] a) J. Suntivich, K. J. May, H. A. Gasteiger, J. B. Goodenough, Y. Shao-Horn, *Science* **2011**, *334*, 1383; b) Q. Yin, J. M. Tan, C. Besson, Y. V. Geletii, D. G. Musaev, A. E. Kuznetsov, Z. Luo, K. I. Hardcastle, C. L. Hill, *Science* **2010**, *328*, 342; c) F. Y. Song, Y. Ding, B. C. Ma, C. M. Wang, Q. Wang, X. Q. Du, S. Fu, J. Song, *Energy Environ. Sci.* **2013**, *6*, 1170; d) S. Cobo, J. Heidkamp, P. A. Jacques, J. Fize, V. Fourmond, L. Guetaz, B. Jousselme, V. Ivanova, H. Dau, S. Palacin, M. Fontecave, V. Artero, *Nat. Mater.* **2012**, *11*, 802; e) M. W. Kanan, D. G. Nocera, *Science* **2008**, *321*, 1072.

[5] a) S. Trasatti, *Electrochim. Acta* **1984**, *29*, 1503; b) S. Ardizzone, G. Fregonara, S. Trasatti, *Electrochim. Acta* **1990**, *35*, 263.

[6] a) Y. Gorlin, T. F. Jaramillo, *J. Am. Chem. Soc.* **2010**, *132*, 13612; b) T. L. Wee, B. D. Sherman, D. Gust, A. L. Moore, T. A. Moore, Y. Liu, J. C. Scaiano, *J. Am. Chem. Soc.* **2011**, *133*, 16742; c) D. K. Bediako, B. Lassalle-Kaiser, Y. Surendranath, J. Yano, V. K. Yachandra, D. G. Nocera, *J. Am. Chem. Soc.* **2012**, *134*, 6801; d) L. Trotochaud, J. K. Ranney, K. N. Williams, S. W. Boettcher, *J. Am. Chem. Soc.* **2012**, *134*, 17253; e) B. S. Yeo, A. T. Bell, *J. Am. Chem. Soc.* **2011**, *133*, 5587; f) A. Grimaud, K. J. May, C. E. Carlton, Y. L. Lee, M. Risch, W. T. Hong, J. Zhou, Y. Shao-Horn, *Nat. Commun.* **2013**, *4*, 2439; g) F. Jiao, H. Frei, *Angew. Chem. Int. Ed.* **2009**, *48*, 1841; *Angew. Chem.* **2009**, *121*, 1873; h) S. Chen, J. Duan, M. Jaroniec, S. Z. Qiao, *Angew. Chem. Int. Ed.* **2013**, *52*, 13567; *Angew. Chem.* **2013**, *125*, 13812.

[7] a) B. S. Yeo, A. T. Bell, *J. Phys. Chem. C* **2012**, *116*, 8394; b) R. Subbaraman, D. Tripkovic, K. C. Chang, D. Strmcnik, A. P. Paulikas, P. Hirunsit, M. Chan, J. Greeley, V. Stamenkovic, N. M. Markovic, *Nat. Mater.* **2012**, *11*, 550; c) B. V. Tilak, P. W. T. Lu, J. E. Colman, S. Srinivasan, *Comprehensive Treatise of Electrochemistry*, Springer, New York, **1981**; d) K. Kinoshita, *Electrochemical Oxygen Technology*, Wiley-Interscience, New York, **1992**; e) M. J. Kenney, M. Gong, Y. G. Li, J. Z. Wu, J. Feng, M. Lanza, H. J. Dai, *Science* **2013**, *342*, 836; f) R. D. Smith, M. S. Prevot, R. D. Fagan, Z. Zhang, P. A. Sedach, M. K. Siu, S. Trudel, C. P. Berlinguette, *Science* **2013**, *340*, 60.

[8] a) Y. Xia, Y. Xiong, B. Lim, S. E. Skrabalak, *Angew. Chem. Int. Ed.* **2009**, *48*, 60; *Angew. Chem.* **2009**, *121*, 62; b) B. T. Qiao, A. Q. Wang, X. F. Yang, L. F. Allard, Z. Jiang, Y. T. Cui, J. Y. Liu, J. Li, T. Zhang, *Nat. Chem.* **2011**, *3*, 634; c) J. M. Yan, X. B. Zhang, S. Han, H. Shioyama, Q. Xu, *Angew. Chem. Int. Ed.* **2008**, *47*, 2287; *Angew. Chem.* **2008**, *120*, 2319; d) P. Huang, J. Lin, W. W. Li, P. F. Rong, Z. Wang, S. J. Wang, X. P. Wang, X. L. Sun, M. Aronova, G. Niu, R. D. Leapman, Z. H. Nie, X. Y. Chen, *Angew. Chem. Int. Ed.* **2013**, *52*, 13958; *Angew. Chem.* **2013**, *125*, 14208; e) S. Sun, G. Zhang, D. Geng, Y. Chen, R. Li, M. Cai, X. Sun, *Angew. Chem. Int. Ed.* **2011**, *50*, 422; *Angew. Chem.* **2011**, *123*, 442.

[9] a) Y. Liang, Y. Li, H. Wang, H. Dai, *J. Am. Chem. Soc.* **2013**, *135*, 2013; b) S. Guo, S. Zhang, L. Wu, S. Sun, *Angew. Chem. Int. Ed.* **2012**, *51*, 11770; *Angew. Chem.* **2012**, *124*, 11940; c) C. Zhang, F. Liu, Y. Zhai, H. Ariga, N. Yi, Y. Liu, K. Asakura, M. Flytzani-Stephanopoulos, H. He, *Angew. Chem. Int. Ed.* **2012**, *51*, 9628; *Angew. Chem.* **2012**, *124*, 9766; d) X. Liu, M. H. Liu, Y. C. Luo, C. Y. Mou, S. D. Lin, H. Cheng, J. M. Chen, J. F. Lee, T. S. Lin, *J. Am. Chem. Soc.* **2012**, *134*, 10251.

[10] a) M. Gong, Y. Li, H. Wang, Y. Liang, J. Z. Wu, J. Zhou, J. Wang, T. Regier, F. Wei, H. Dai, *J. Am. Chem. Soc.* **2013**, *135*, 8452; b) M. R. Gao, Y. F. Xu, J. Jiang, Y. R. Zheng, S. H. Yu, *J. Am. Chem. Soc.* **2012**, *134*, 2930; c) Y. Liang, Y. Li, H. Wang, J. Zhou, J. Wang, T. Regier, H. Dai, *Nat. Mater.* **2011**, *10*, 780; d) Y. Gorlin, C. J. Chung, J. D. Benck, D. Nordlund, L. Seitz, T. C. Weng, D. Sokaras, B. M. Clemens, T. F. Jaramillo, *J. Am. Chem. Soc.* **2014**, *136*, 4920.

[11] a) R. Bashyam, P. Zelenay, *Nature* **2006**, *443*, 63; b) G. Wu, K. L. More, C. M. Johnston, P. Zelenay, *Science* **2011**, *332*, 443; c) M. Lefevre, E. Proietti, F. Jaouen, J. P. Dodelet, *Science* **2009**, *324*, 71.

[12] a) N. Ramaswamy, U. Tylus, Q. Jia, S. Mukerjee, *J. Am. Chem. Soc.* **2013**, *135*, 15443; b) U. Tylus, Q. Jia, K. Strickland, N. Ramaswamy, A. Serov, P. Atanassov, S. Mukerjee, *J. Phys. Chem. C* **2014**, *118*, 8999.

[13] a) H. Lee, S. M. Dellatore, W. M. Miller, P. B. Messersmith, *Science* **2007**, *318*, 426; b) Y. Liu, K. Ai, L. Lu, *Chem. Rev.* **2014**, *114*, 5057.

[14] S. Pintado, S. Goberna-Ferron, E. C. Escudero-Adan, J. R. Galan-Mascaros, *J. Am. Chem. Soc.* **2013**, *135*, 13270.

[15] a) Y. Surendranath, M. W. Kanan, D. G. Nocera, *J. Am. Chem. Soc.* **2010**, *132*, 16501; b) M. Dincă, Y. Surendranath, D. G. Nocera, *Proc. Natl. Acad. Sci. USA* **2010**, *107*, 10337; c) Z. Chen, A. R. Rathmell, S. Ye, A. R. Wilson, B. J. Wiley, *Angew. Chem. Int. Ed.* **2013**, *52*, 13708; *Angew. Chem.* **2013**, *125*, 13953; d) C. C. McCrory, S. Jung, J. C. Peters, T. F. Jaramillo, *J. Am. Chem. Soc.* **2013**, *135*, 16977; e) X. Zou, A. Goswami, T. Asefa, *J. Am. Chem. Soc.* **2013**, *135*, 17242; f) Y. Zhao, R. Nakamura, K. Kamiya, S. Nakanishi, K. Hashimoto, *Nat. Commun.* **2013**, *4*, 2390.

[16] a) M. A. Peck, M. A. Langell, *Chem. Mater.* **2012**, *24*, 4483; b) M. C. Biesinger, B. P. Payne, L. W. M. Lau, A. Gerson, R. S. C. Smart, *Surf. Interface Anal.* **2009**, *41*, 324.

[17] M. L. Fdez-Gubieda, A. Muela, J. Alonso, A. García-Prieto, L. Olivi, R. Fernández-Pacheco, J. M. Barandiarán, *ACS Nano* **2013**, *7*, 3297.

Received: May 13, 2015
Published online: July 14, 2015

